Chapter 19
Bose-Einstein Condensation

Abstract Bose-Einstein condensation (BEC) refers to a prediction of quantum statistical mechanics (Bose [1], Einstein [2]) where an ideal gas of identical bosons undergoes a phase transition when the thermal de Broglie wavelength exceeds the mean spacing between the particles. Under these conditions, bosons are stimulated by the presence of other bosons in the lowest energy state to occupy that state as well, resulting in a macroscopic occupation of a single quantum state. The condensate that forms constitutes a macroscopic quantum-mechanical object. BEC was first observed in 1995, seventy years after the initial predictions, and resulted in the award of 2001 Nobel Prize in Physics to Cornell, Ketterle and Weiman. The experimental observation of BEC was achieved in a dilute gas of alkali atoms in a magnetic trap. The first experiments used ^{87}Rb atoms [3], ^{23}Na [4], ^{7}Li [5], and H [6] more recently metastable He has been condensed [7]. The list of BEC atoms now includes molecular systems such as Rb_2 [8], Li_2 [9] and Cs_2 [10]. In order to cool the atoms to the required temperature ($\sim$200 nK) and densities (10^{13}–10^{14} cm^{-3}) for the observation of BEC a combination of optical cooling and evaporative cooling were employed. Early experiments used magnetic traps but now optical dipole traps are also common. Condensates containing up to 5×10^{9} atoms have been achieved for atoms with a positive scattering length (repulsive interaction), but small condensates have also been achieved with only a few hundred atoms. In recent years Fermi degenerate gases have been produced [11], but we will not discuss these in this chapter.

BECs are now routinely produced in dozens of laboratories around the world. They have provided a wonderful test bed for condensed matter physics with stunning experimental demonstrations of, among other things, interference between condensates, superfluidity and vortices. More recently they have been used to create optically nonlinear media to demonstrate electromagnetically induced transparency and neutral atom arrays in an optical lattice via a Mott insulator transition.

Many experiments on BECs are well described by a semiclassical theory discussed below. Typically these involve condensates with a large number of atoms, and in some ways are analogous to describing a laser in terms of a semiclassical mean field. More recent experiments however have begun to probe quantum

properties of the condensate, and are related to the fundamental discreteness of the field and nonlinear quantum dynamics. In this chapter, we discuss some of these quantum properties of the condensate. We shall make use of "few mode" approximations which treat only essential condensate modes and ignore all noncondensate modes. This enables us to use techniques developed for treating quantum optical systems described in earlier chapters of this book.

19.1 Hamiltonian: Binary Collision Model

The effects of interparticle interactions are of fundamental importance in the study of dilute–gas Bose–Einstein condensates. Although the actual interaction potential between atoms is typically very complex, the regime of operation of current experiments is such that interactions can in fact be treated very accurately with a much–simplified model. In particular, at very low temperature the de Broglie wavelengths of the atoms are very large compared to the range of the interatomic potential. This, together with the fact that the density and energy of the atoms are so low that they rarely approach each other very closely, means that atom–atom interactions are effectively *weak* and dominated by (elastic) *s*–wave scattering. It follows also that to a good approximation one need only consider *binary* collisions (i.e., three–body processes can be neglected) in the theoretical model.

The *s*–wave scattering is characterised by the *s*–wave scattering length, a, the sign of which depends sensitively on the precise details of the interatomic potential [$a > 0$ ($a < 0$) for repulsive (attractive) interactions]. Given the conditions described above, the interaction potential can be approximated by

$$U(\mathbf{r}-\mathbf{r}') = U_0\delta(\mathbf{r}-\mathbf{r}') \,, \tag{19.1}$$

(i.e., a hard sphere potential) with U_0 the interaction "strength," given by

$$U_0 = \frac{4\pi\hbar^2 a}{m} \,, \tag{19.2}$$

and the Hamiltonian for the system of weakly interacting bosons in an external potential, $V_{\rm trap}(\mathbf{r})$, can be written in the second quantised form as

$$\begin{aligned}\hat{H} = &\int \mathrm{d}^3 r\, \hat{\Psi}^\dagger(\mathbf{r}) \left[-\frac{\hbar^2}{2m}\nabla^2 + V_{\rm trap}(\mathbf{r})\right] \hat{\Psi}(\mathbf{r}) \\ &+\frac{1}{2}\int \mathrm{d}^3 r \int \mathrm{d}^3 r' \hat{\Psi}^\dagger(\mathbf{r})\hat{\Psi}^\dagger(\mathbf{r}')U(\mathbf{r}-\mathbf{r}')\hat{\Psi}(\mathbf{r}')\hat{\Psi}(\mathbf{r})\end{aligned} \tag{19.3}$$

where $\hat{\Psi}(\mathbf{r})$ and $\hat{\Psi}^\dagger(\mathbf{r})$ are the boson field operators that annihilate or create a particle at the position $\mathbf{r}$, respectively.

To put a quantitative estimate on the applicability of the model, if ρ is the density of bosons, then a necessary condition is that $a^3\rho \ll 1$ (for $a > 0$). This condition is indeed satisfied in the alkali gas BEC experiments [3, 4], where achieved densities of the order of $10^{12} - 10^{13}$ cm^{-3} correspond to $a^3\rho \simeq 10^{-5} - 10^{-6}$.

19.2 Mean–Field Theory — Gross-Pitaevskii Equation

The Heisenberg equation of motion for $\hat{\Psi}(\mathbf{r})$ is derived as

$$\mathrm{i}\hbar\frac{\partial\hat{\Psi}(\mathbf{r},t)}{\partial t} = \left[-\frac{\hbar^2}{2m}\nabla^2 + V_{\mathrm{trap}}(\mathbf{r})\right]\hat{\Psi}(\mathbf{r},t) + U_0\hat{\Psi}^\dagger(\mathbf{r},t)\hat{\Psi}(\mathbf{r},t)\hat{\Psi}(\mathbf{r},t)\,, \qquad (19.4)$$

which cannot in general be solved. In the mean–field approach, however, the expectation value of (19.4) is taken and the field operator decomposed as

$$\hat{\Psi}(\mathbf{r},t) = \Psi(\mathbf{r},t) + \tilde{\Psi}(\mathbf{r},t)\,, \qquad (19.5)$$

where $\Psi(\mathbf{r},t) = \langle\hat{\Psi}(\mathbf{r},t)\rangle$ is the "condensate wave function" and $\tilde{\Psi}(\mathbf{r})$ describes quantum and thermal fluctuations around this mean value. The quantity $\Psi(\mathbf{r},t)$ is in fact a classical field possessing a well–defined phase, reflecting a broken gauge symmetry associated with the condensation process. The expectation value of $\tilde{\Psi}(\mathbf{r},t)$ is zero and, in the mean–field theory, its effects are assumed to be small, amounting to the assumption of the thermodynamic limit, where the number of particles tends to infinity while the density is held fixed. For the effects of $\tilde{\Psi}(\mathbf{r})$ to be *negligibly small* in the equation for $\Psi(\mathbf{r})$ also amounts to an assumption of zero temperature (i.e., pure condensate). Given that this is so, and using the normalisation

$$\int \mathrm{d}^3r\,|\Psi(\mathbf{r},t)|^2 = 1\,, \qquad (19.6)$$

one is lead to the nonlinear Schrödinger equation, or "Gross–Pitaevskii equation" (GP equation), for the condensate wave function $\Psi(\mathbf{r},t)$ [13],

$$\mathrm{i}\hbar\frac{\partial\Psi(\mathbf{r},t)}{\partial t} = \left[-\frac{\hbar^2}{2m}\nabla^2 + V_{\mathrm{trap}}(\mathbf{r}) + NU_0|\Psi(\mathbf{r},t)|^2\right]\Psi(\mathbf{r},t)\,, \qquad (19.7)$$

where N is the mean number of particles in the condensate. The nonlinear interaction term (or mean–field pseudo–potential) is proportional to the number of atoms in the condensate and to the s–wave scattering length through the parameter U_0.

A stationary solution for the condensate wavefunction may be found by substituting $\psi(\mathbf{r},t) = \exp\left(\frac{-\mathrm{i}\mu t}{\hbar}\right)\psi(\mathbf{r})$ into (19.7) (where μ is the chemical potential of the condensate). This yields the time independent equation,

$$\left[\frac{-\hbar^2}{2m}\nabla^2 + V_{\rm trap}(\mathbf{r}) + NU_0\,|\psi(\mathbf{r})|^2\right]\psi(\mathbf{r}) = \mu\,\psi(\mathbf{r}) \ . \tag{19.8}$$

The GP equation has proved most successful in describing many of the mean field properties of the condensate. The reader is referred to the review articles listed in further reading for a comprehensive list of references. In this chapter we shall focus on the quantum properties of the condensate and to facilitate our investigations we shall go to a single mode model.

19.3 Single Mode Approximation

The study of the quantum statistical properties of the condensate (at $T = 0$) can be reduced to a relatively simple model by using a mode expansion and subsequent truncation to just a single mode (the "condensate mode"). In particular, one writes the Heisenberg atomic field annihilation operator as a mode expansion over single–particle states,

$$\begin{aligned}\hat{\Psi}(\mathbf{r},t) &= \sum_\alpha a_\alpha(t)\psi_\alpha(\mathbf{r})\exp^{-{\rm i}\mu_\alpha t/\hbar} \\ &= a_0(t)\psi_0(\mathbf{r})\exp^{-{\rm i}\mu_0 t/\hbar} + \tilde{\Psi}(\mathbf{r},t)\ ,\end{aligned} \tag{19.9}$$

where $[a_\alpha(t), a^\dagger_\beta(t)] = \delta_{\alpha\beta}$ and $\{\psi_\alpha(\mathbf{r})\}$ are a complete orthonormal basis set and $\{\mu_\alpha\}$ the corresponding eigenvalues. The first term in the second line of (19.9) acts only on the condensate state vector, with $\psi_0(\mathbf{r})$ chosen as a solution of the stationary GP equation (19.8) (with chemical potential μ_0 and mean number of condensate atoms N). The second term, $\tilde{\Psi}(\mathbf{r},t)$, accounts for non–condensate atoms. Substituting this mode expansion into the Hamiltonian

$$\begin{aligned}\hat{H} = &\int {\rm d}^3 r\,\hat{\Psi}^\dagger(\mathbf{r})\left[-\frac{\hbar^2}{2m}\nabla^2 + V_{\rm trap}(\mathbf{r})\right]\hat{\Psi}(\mathbf{r}) \\ &+(U_0/2)\int {\rm d}^3 r\,\hat{\Psi}^\dagger(\mathbf{r})\hat{\Psi}^\dagger(\mathbf{r})\hat{\Psi}(\mathbf{r})\hat{\Psi}(\mathbf{r})\ ,\end{aligned} \tag{19.10}$$

and retaining only condensate terms, one arrives at the single–mode effective Hamiltonian

$$\hat{H} = \hbar\tilde{\omega}_0 a_0^\dagger a_0 + \hbar\kappa a_0^\dagger a_0^\dagger a_0 a_0\ , \tag{19.11}$$

where

$$\hbar\tilde{\omega}_0 = \int {\rm d}^3 r\,\psi_0^*(\mathbf{r})\left[-\frac{\hbar^2}{2m}\nabla^2 + V_{\rm trap}(\mathbf{r})\right]\psi_0(\mathbf{r})\ , \tag{19.12}$$

and

$$\hbar\kappa = \frac{U_0}{2}\int {\rm d}^3 r\,|\psi_0(\mathbf{r})|^4\ . \tag{19.13}$$

We have assumed that the state is prepared slowly, with damping and pumping rates vanishingly small compared to the trap frequencies and collision rates. This means that the condensate remains in thermodynamic equilibrium throughout its preparation. Finally, the atom number distribution is assumed to be sufficiently narrow that the parameters $\tilde{\omega}_0$ and κ, which of course depend on the atom number, can be regarded as constants (evaluated at the mean atom number). In practice, this proves to be a very good approximation.

19.4 Quantum State of the Condensate

A Bose-Einstein condensate (BEC) is often viewed as a coherent state of the atomic field with a definite phase. The Hamiltonian for the atomic field is independent of the condensate phase (see Exercise 19.1) so it is often convenient to invoke a symmetry breaking Bogoliubov field to select a particular phase. In addition, a coherent state implies a superposition of number states, whereas in a single trap experiment there is a fixed number of atoms in the trap (even if we are ignorant of that number) and the state of a simple trapped condensate must be a number state (or, more precisely, a mixture of number states as we do not know the number in the trap from one preparation to the next). These problems may be bypassed by considering a system of two condensates for which the total number of atoms N is fixed. Then, a general state of the system is a superposition of number difference states of the form,

$$|\psi\rangle = \sum_{k=0}^{N} c_k \, |k, N-k\rangle \tag{19.14}$$

As we have a well defined superposition state, we can legitimately consider the relative phase of the two condensates which is a Hermitian observable. We describe in Sect. 19.6 how a particular relative phase is established due to the measurement process.

The identification of the condensate state as a coherent state must be modified in the presence of collisions except in the case of very strong damping.

19.5 Quantum Phase Diffusion: Collapses and Revivals of the Condensate Phase

The macroscopic wavefunction for the condensate for a relatively strong number of atoms will exhibit collapses and revivals arising from the quantum evolution of an initial state with a spread in atom number [21]. The initial collapse has been described as quantum phase diffusion [20]. The origins of the collapses and revivals may be seen straightforwardly from the single–mode model. From the Hamiltonian

$$\hat{H} = \hbar\tilde{\omega}_0 a_0^\dagger a_0 + \hbar\kappa a_0^\dagger a_0^\dagger a_0 a_0 \,, \tag{19.15}$$

the Heisenberg equation of motion for the condensate mode operator follows as

$$\begin{aligned} \dot{a}_0(t) &= -\frac{\mathrm{i}}{\hbar}[a_0, H] \\ &= -\mathrm{i}\left(\tilde{\omega}_0 a_0 + 2\kappa a_0^\dagger a_0 a_0\right) \,, \end{aligned} \tag{19.16}$$

for which a solution can be written in the form

$$a_0(t) = \exp\left[-\mathrm{i}\left(\tilde{\omega}_0 + 2\kappa a_0^\dagger a_0\right) t\right] a_0(0) \,. \tag{19.17}$$

Writing the initial state of the condensate, $|i\rangle$, as a superposition of number states,

$$|i\rangle = \sum_n c_n |n\rangle \,, \tag{19.18}$$

the expectation value $\langle i|a_0(t)|i\rangle$ is given by

$$\begin{aligned} \langle i|a_0(t)|i\rangle &= \sum_n c_{n-1}^* c_n \sqrt{n}\, \exp\{-\mathrm{i}\,[\tilde{\omega}_0 + 2\kappa(n-1)]t\} \\ &= \sum_n c_{n-1}^* c_n \sqrt{n}\, \exp\left(-\frac{\mathrm{i}\mu t}{\hbar}\right) \exp\{-2\mathrm{i}\kappa(n-N)t\} \,, \end{aligned} \tag{19.19}$$

where the relationship

$$\mu = \hbar\tilde{\omega}_0 + 2\hbar\kappa(N-1) \,, \tag{19.20}$$

has been used [this expression for μ uses the approximation $\langle n^2\rangle = N^2 + (\Delta n)^2 \approx N^2$]. The factor $\exp(-\mathrm{i}\mu t/\hbar)$ describes the deterministic motion of the condensate mode in phase space and can be removed by transforming to a rotating frame of reference, allowing one to write

$$\langle i|a_0(t)|i\rangle = \sum_n c_{n-1}^* c_n \sqrt{n}\, \{\cos[2\kappa(n-N)t] - \mathrm{i}\sin[2\kappa(n-N)t]\} \,. \tag{19.21}$$

This expression consists of a weighted sum of trigonometric functions with different frequencies. With time, these functions alternately "dephase" and "rephase," giving rise to collapses and revivals, respectively, in analogy with the behaviour of the Jaynes–Cummings Model of the interaction of a two–level atom with a single electromagnetic field mode described in Sect. 10.2. The period of the revivals follows directly from (19.21) as $T = \pi/\kappa$. The collapse time can be derived by considering the spread of frequencies for particle numbers between $n = N + (\Delta n)$ and $n = N - (\Delta n)$, which yields $(\Delta\Omega) = 2\kappa(\Delta n)$; from this one estimates $t_{\mathrm{coll}} \simeq 2\pi/(\Delta\Omega) = T/(\Delta n)$, as before.

From the expression $t_{\mathrm{coll}} \simeq T/(\Delta n)$, it follows that the time taken for collapse depends on the statistics of the condensate; in particular, on the "width" of the initial distribution. This dependence is illustrated in Fig. 19.1, where the real part of $\langle a_0(t)\rangle$

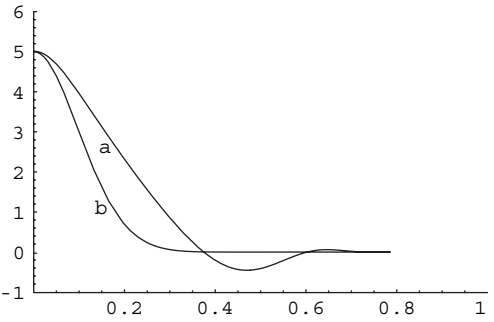

Fig. 19.1 The real part of the condensate amplitude versus time, $\mathrm{Re}\{\langle a_0(t)\rangle\}$ for an amplitude–squeezed state, (**a**) and a coherent state (**b**) with the same mean number of atoms, $N = 25$

is plotted as a function of time for two different initial states: (a) an amplitude–squeezed state, (b) a coherent state. The mean number of atoms is chosen in each case to be $N = 25$.

The timescales of the collapses show clear differences; the more strongly number–squeezed the state is, the longer its collapse time. The revival times, however, are independent of the degree of number squeezing and depend only on the interaction parameter, κ. For example, a condensate of Rb 2,000 atoms with the $\omega/2\pi = 60\,\mathrm{Hz}$, has revival time of approximately 8 s, which lies within the typical lifetime of the experimental condensate (10–20 s).

One can examine this phenomenon in the context of the interference between a pair of condensates and indeed one finds that the visibility of the interference pattern also exhibits collapses and revivals, offering an alternative means of detecting this effect. To see this, consider, as above, that atoms are released from two condensates with momenta k_1 and k_2 respectively. Collisions within each condensate are described by the Hamiltonian (neglecting cross–collisions)

$$\hat{H} = \hbar\kappa\left[\left(a_1^\dagger a_1\right)^2 + \left(a_2^\dagger a_2\right)^2\right] , \tag{19.22}$$

from which the intensity at the detector follows as

$$\begin{aligned} I(x,t) &= I_0\langle[a_1^\dagger(t)\exp^{\mathrm{i}k_1 x} + a_2^\dagger(t)\exp^{\mathrm{i}k_2 x}][a_1(t)\exp^{-\mathrm{i}k_1 x} + a_2(t)\exp^{-\mathrm{i}k_2 x}]\rangle \\ &= I_0\Big\{\langle a_1^\dagger a_1\rangle + \langle a_2^\dagger a_2\rangle \\ &\quad + \langle a_1^\dagger \exp\left[2\mathrm{i}\left(a_1^\dagger a_1 - a_2^\dagger a_2\right)\kappa t\right] a_2\rangle\exp^{-\mathrm{i}\phi(x)} + \mathrm{h.c.}\Big\} , \end{aligned} \tag{19.23}$$

where $\phi(x) = (k_2 - k_1)x$.

If one assumes that each condensate is initially in a coherent state of amplitude $|\alpha|$, with a relative phase ϕ between the two condensates, i.e., assuming that

$$|\varphi(t=0)\rangle = |\alpha\rangle|\alpha e^{-\mathrm{i}\phi}\rangle , \tag{19.24}$$

then one obtains for the intensity

$$I(x,t) = I_0 \frac{|\alpha|^2}{2} \left\{1 + \exp\left[2|\alpha|^2 (\cos(2\kappa t) - 1)\right] \cos\left[\phi(x) - \phi\right]\right\} . \tag{19.25}$$

From this expression, it is clear that the visibility of the interference pattern undergoes collapses and revivals with a period equal to π/κ. For short times $t \ll 1/2\kappa$, this can be written as

$$I(x,t) = I_0 \frac{|\alpha|^2}{2} \left[1 + \exp\left(-|\alpha|^2 \kappa^2 t^2\right)\right] , \tag{19.26}$$

from which the collapse time can be identified as $t_{\text{coll}} = 1/\kappa|\alpha|$.

An experimental demonstration of the collapse and revival of a condensate was done by the group of Bloch in 2002 [12]. In the experiment coherent states of ^{87}Rb atoms were prepared in a three dimensional optical lattice where the tunneling is larger than the on-site repulsion. The condensates in each well were phase coherent with constant relative phases between the sites, and the number distribution in each well is close to Poisonnian. As the optical dipole potential is increased the depth of the potential wells increases and the inter-well tunneling decreases producing a sub-Poisson number distribution in each well due to the repulsive interaction between the atoms. After preparing the states in each well, the well depth is rapidly increased to create isolated potential wells. The nonlinear interaction of (19.15) then determines the dynamics in each well. After some time interval, the *hold time*, the condensate is released from the trap and the resulting interference pattern is imaged. As the mean field amplitude in each well undergoes a collapse the resulting interference pattern visibility decreases. However as the mean field revives, the visibility of the interference pattern also revives. The experimental results are shown in Fig. 19.2.

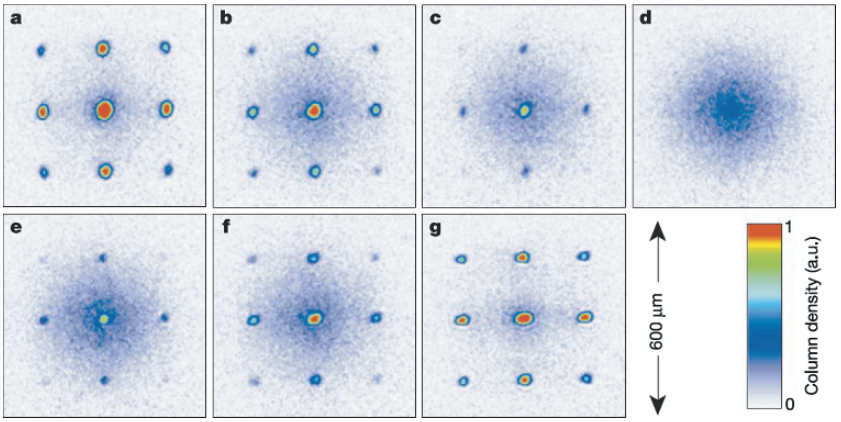

Fig. 19.2 The interference pattern imaged from the released condensate after different hold times. In (**d**) the interference fringes have entirely vanished indicating a complete collapse of the amplitude of the condensate. In (**g**), the wait time is now close to the complete revival time for the coherent amplitude and the fringe pattern is restored. From Fig. 2 of [12]

19.6 Interference of Two Bose–Einstein Condensates and Measurement–Induced Phase

The standard approach to a Bose–Einstein condensate assumes that it exhibits a well–defined *amplitude*, which unavoidably introduces the condensate *phase*. Is this phase just a formal construct, not relevant to any real measurement, or can one actually observe something in an experiment? Since one needs a phase reference to observe a phase, two options are available for investigation of the above question. One could compare the condensate phase to itself at a different time, thereby examining the condensate phase dynamics, or one could compare the phases of two distinct condensates. This second option has been studied by a number of groups, pioneered by the work of Javanainen and Yoo [23] who consider a pair of statistically independent, physically–separated condensates allowed to drop and, by virtue of their horizontal motion, overlap as they reach the surface of an atomic detector. The essential result of the analysis is that, even though no phase information is initially present (the initial condensates may, for example, be in number states), an interference pattern may be formed and a relative phase established as a result of the measurement. This result may be regarded as a constructive example of spontaneous symmetry breaking. Every particular measurement produces a certain relative phase between the condensates; however, this phase is random, so that the symmetry of the system, being broken in a *single measurement*, is restored if an *ensemble of measurements* is considered.

The physical configuration we have just described and the predicted interference between two overlapping condensates was realised in a beautiful experiment performed by Andrews et al. [18] at MIT. The observed fringe pattern is shown in Fig. 19.8.

19.6.1 Interference of Two Condensates Initially in Number States

To outline this effect, we follow the working of Javanainen and Yoo [23] and consider two condensates made to overlap at the surface of an atom detector. The condensates each contain $N/2$ (noninteracting) atoms of momenta k_1 and k_2, respectively, and in the detection region the appropriate field operator is

$$\hat{\psi}(x) = \frac{1}{\sqrt{2}}\left[a_1 + a_2 \exp^{i\phi(x)}\right] , \tag{19.27}$$

where $\phi(x) = (k_2 - k_1)x$ and a_1 and a_2 are the atom annihilation operators for the first and second condensate, respectively. For simplicity, the momenta are set to $\pm\pi$, so that $\phi(x) = 2\pi x$. The initial state vector is represented simply by

$$|\varphi(0)\rangle = |N/2, N/2\rangle . \tag{19.28}$$

Assuming *destructive* measurement of atomic position, whereby none of the atoms interacts with the detector twice, a direct analogy can be drawn with the theory of absorptive photodetection and the joint counting rate R^m for m atomic detections at positions $\{x_1,\cdots,x_m\}$ and times $\{t_1,\cdots,t_m\}$ can be defined as the normally–ordered average

$$\begin{aligned} R^m \;& (x_1,t_1,\ldots,x_m,t_m) \\ &= K^m\langle\hat{\psi}^\dagger(x_1,t_1)\cdots\hat{\psi}^\dagger(x_m,t_m)\hat{\psi}(x_m,t_m)\cdots\hat{\psi}(x_1,t_1)\rangle\ . \end{aligned} \tag{19.29}$$

Here, K^m is a constant that incorporates the sensitivity of the detectors, and $R^m=0$ if $m>N$, i.e., no more than N detections can occur.

Further assuming that all atoms are in fact detected, the *joint probability density* for detecting m atoms at positions $\{x_1,\cdots,x_m\}$ follows as

$$p^m(x_1,\cdots,x_m)=\frac{(N-m)!}{N!}\langle\hat{\psi}^\dagger(x_1)\cdots\hat{\psi}^\dagger(x_m)\hat{\psi}(x_m)\cdots\hat{\psi}(x_1)\rangle \tag{19.30}$$

The *conditional probability density*, which gives the probability of detecting an atom at the position x_m given $m-1$ previous detections at positions $\{x_1,\cdots,x_{m-1}\}$, is defined as

$$p(x_m|x_1,\cdots,x_{m-1})=\frac{p^m(x_1,\cdots,x_m)}{p^{m-1}(x_1,\cdots,x_{m-1})}\ , \tag{19.31}$$

and offers a straightforward means of directly simulating a sequence of atom detections [23, 24]. This follows from the fact that, by virtue of the form for $p^m(x_1,\cdots,x_m)$, the conditional probabilities can all be expressed in the simple form

$$p(x_m|x_1,\cdots,x_{m-1})=1+\beta\cos(2\pi x_m+\varphi)\ , \tag{19.32}$$

where β and φ are parameters that depend on $\{x_1,\cdots,x_{m-1}\}$. The origin of this form can be seen from the action of each measurement on the previous result,

$$\langle\varphi_m|\hat{\psi}^\dagger(x)\hat{\psi}(x)|\varphi_m\rangle=(N-m)+2A\cos[\theta-\phi(x)]\ , \tag{19.33}$$

with $A\exp^{-i\theta}=\langle\varphi_m|a_1^\dagger a_2|\varphi_m\rangle$.

So, to simulate an experiment, one begins with the distribution $p^1(x)=1$, i.e., one chooses the first random number (the position of the first atom detection), x_1, from a uniform distribution in the interval $[0,1]$ (obviously, before any measurements are made, there is no information about the phase or visibility of the interference). After this "measurement," the state of the system is

$$\begin{aligned} |\varphi_1\rangle \;&= \hat{\psi}(x_1)|\varphi_0\rangle \\ &= \sqrt{N/2}\left\{|(N/2)-1,N/2\rangle+|N/2,(N/2)-1\rangle\exp^{i\phi(x_1)}\right\}\ . \end{aligned} \tag{19.34}$$

That is, one now has an entangled state containing phase information due to the fact that one does not know from which condensate the detected atom came. The corresponding conditional probability density for the second detection can be derived as

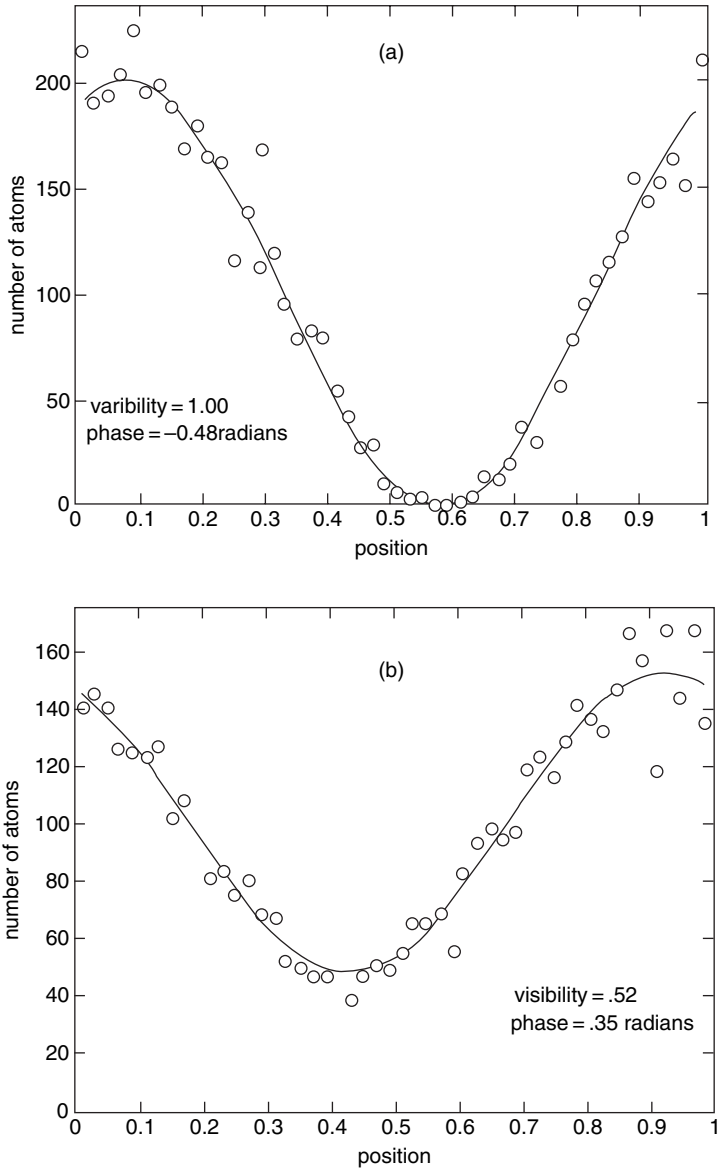

Fig. 19.3 (**a**) Numerical simulation of $5,000$ atomic detections for $N = 10,000$ (circles). The solid curve is a least-squares fit using the function $1 + \beta \cos(2\pi x + \varphi)$. The free parameters are the visibility β and the phase φ. The detection positions are sorted into 50 equally spaced bins. (**b**) Collisions included ($\kappa = 2\gamma$ giving a visibility of about one-half of the no collision case. From Wong et al. [24]

$$p(x|x_1) = \frac{p^2(x_1,x)}{p^1(x_1)} = \frac{1}{N-1}\,\frac{\langle\hat{\psi}^\dagger(x_1)\hat{\psi}^\dagger(x)\hat{\psi}(x)\hat{\psi}(x_1)\rangle}{\langle\hat{\psi}^\dagger(x_1)\hat{\psi}(x_1)\rangle} \tag{19.35}$$

$$= \frac{1}{2}\left\{1+\frac{N}{2(N-1)}\cos\left[\phi(x)-\phi(x_1)\right]\right\}. \tag{19.36}$$

Hence, after just one measurement the visibility (for large N) is already close to $1/2$, with the phase of the interference pattern dependent on the first measurement x_1. The second position, x_2, is chosen from the distribution (19.36). The conditional probability $p(x|x_1)$ has, of course, the form (19.32), with β and φ taking simple analytic forms. However, expressions for β and φ become more complicated with increasing m, and in practice the approach one takes is to simply calculate $p(x|x_1,\cdots,x_{m-1})$ numerically for two values of x [using the form (19.30) for $p^m(x_1,\ldots,x_{m-1},x)$, and noting that $p^{m-1}(x_1,\ldots,x_{m-1})$ is simply a number already determined by the simulation] and then, using these values, solve for β and φ. This then defines exactly the distribution from which to choose x_m.

The results of simulations making use of the above procedure are shown in Figs 19.3 – 19.4. Figure 19.3 shows a histogram of 5,000 atom detections from condensates initially containing $N/2 = 5{,}000$ atoms each with and without collisions. From a fit of the data to a function of the form $1+\beta\cos(2\pi x+\varphi)$, the visibility of the interference pattern, β, is calculated to be 1. The conditional probability distributions calculated before each detection contain what one can define as a *con-*

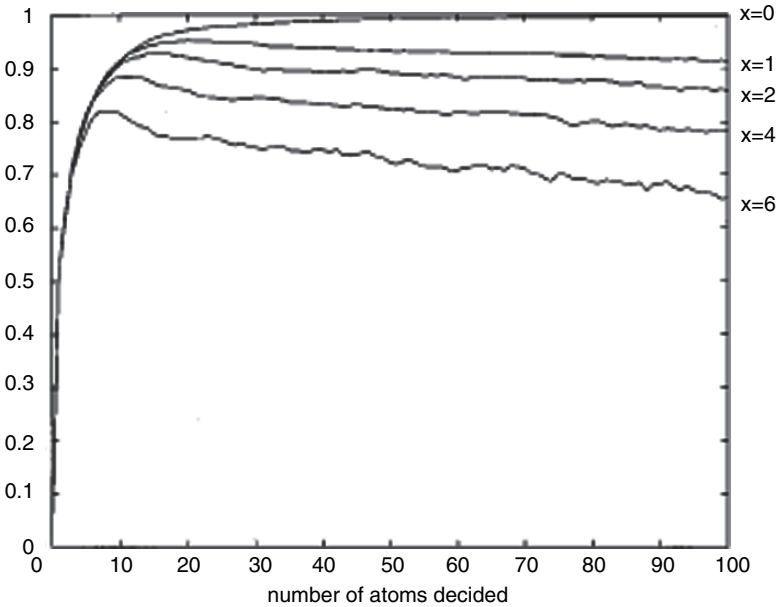

Fig. 19.4 Averaged conditional visibility as a function of the number of detected atoms. From Wong et al. [13]

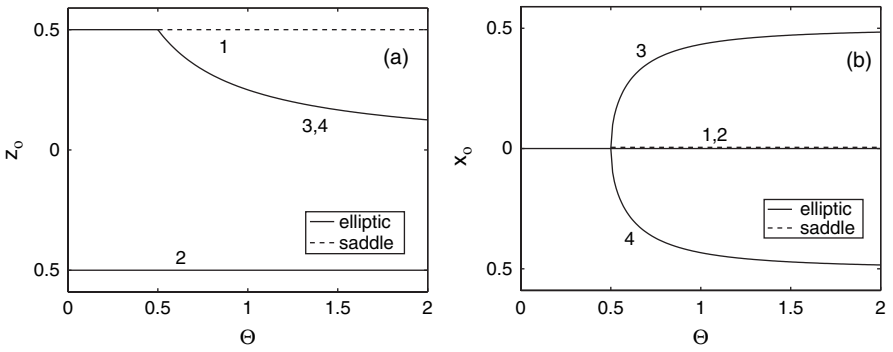

Fig. 19.5 Fixed point bifurcation diagram of the two mode semiclassical BEC dynamics. (**a**) z^*, (**b**) x^* . *Solid line* is stable while *dashed line* is unstable.

ditional visibility. Following the value of this conditional visibility gives a quantitative measure of the buildup of the interference pattern as a function of the number of detections. The conditional visibility, averaged over many simulations, is shown as a function of the number of detections in Fig. 19.4 for $N = 200$. One clearly sees the sudden increase to a value of approximately 0.5 after the first detection, followed by a steady rise towards the value 1.0 (in the absence of collisions) as each further detection provides more information about the phase of the interference pattern.

One can also follow the evolution of the *conditional phase* contained within the conditional probability distribution. The final phase produced by each individual simulation is, of course, random but the trajectories are seen to stabilise about a particular value after approximately 50 detections (for $N = 200$).

19.7 Quantum Tunneling of a Two Component Condensate

A two component condensate in a double well potential is a non trivial nonlinear dynamical model. Suppose the trapping potential in (19.3) is given by

$$V(\mathbf{r}) = b(x^2 - q_0^2)^2 + \frac{1}{2}m\omega_t^2(y^2 + z^2) \tag{19.37}$$

where ω_t is the trap frequency in the y–z plane. The potential has elliptic fixed points at $\mathbf{r}_1 = +q_0\mathbf{x}$, $\mathbf{r}_2 = -q_0\mathbf{x}$ near which the linearised motion is harmonic with frequency $\omega_0 = q_o\,(8b/m)^{1/2}$. For simplicity we set $\omega_t = \omega_0$ and scale the length in units of $r_0 = \sqrt{\hbar/2m\omega_0}$, which is the position uncertainty in the harmonic oscillator ground state. The barrier height is $B = (\hbar\omega/8)(q_0/r_0)^2$. We can justify a two mode expansion of the condensate field by assuming the potential parameters are chosen so that the two lowest single particle energy eigenstates are below the barrier, with

the next highest energy eigenstate separated from the ground state doublet by a large gap. We will further assume that the interaction term is sufficiently weak that, near zero temperature, the condensate wave functions are well approximated by the single particle wave functions.

The potential may be expanded around the two stable fixed points to quadratic order

$$V(\mathbf{r}) = \tilde{V}^{(2)}(\mathbf{r}-\mathbf{r}_j) + \dots \tag{19.38}$$

where $j = 1,2$ and

$$\tilde{V}^{(2)}(\mathbf{r}) = 4bq_0^2|\mathbf{r}|^2 \tag{19.39}$$

We can now use as the local mode functions the single particle wave functions for harmonic oscillators ground states, with energy E_0, localised in each well,

$$u_j(\mathbf{r}) = \frac{-(-1)^j}{(2\pi r_0^2)^{3/4}} \exp\left[-\frac{1}{4}((x-q_0)^2+y^2+z^2)/r_0^2\right] \tag{19.40}$$

These states are almost orthogonal, with the deviation from orthogonality given by the overlap under the barrier,

$$\int \mathrm{d}^3\mathbf{r} u_j^*(\mathbf{r})u_k(\mathbf{r}) = \delta_{j,k} + (1-\delta_{j,k})\varepsilon \tag{19.41}$$

with $\varepsilon = \mathrm{e}^{-\frac{1}{2}q_0^2/r_0^2}$.

The localised states in (19.40) may be used to approximate the single particle energy (and parity) eigenstates as

$$u_\pm \approx \frac{1}{\sqrt{2}}[u_1(\mathbf{r}) \pm u_2(\mathbf{r})] \tag{19.42}$$

corresponding to the energy eigenvalues $E_\pm = E_0 \pm \mathscr{R}$ with

$$\mathscr{R} = \int \mathrm{d}^3\mathbf{r}\; u_1^*(\mathbf{r})[V(\mathbf{r}) - \tilde{V}(\mathbf{r}-\mathbf{r}_1)]u_2(\mathbf{r}) \tag{19.43}$$

A localised state is thus an even or odd superposition of the two lowest energy eigenstates. Under time evolution the relative phase of the superposition can change sign after a time $T = 2\pi/\Omega$, the tunneling time, where the tunneling frequency is given by

$$\Omega = \frac{2\mathscr{R}}{\hbar} = \frac{3}{8}\omega_0 \frac{q_0^2}{r_0^2}\, e^{-q_0^2/2r_0^2} \tag{19.44}$$

We now make the two-mode approximation by expanding the field operator as

$$\hat{\psi}(\mathbf{r},t) = c_1(t)\; u_1(\mathbf{r}) + c_2(t)\; u_2(\mathbf{r}) \tag{19.45}$$

where

$$c_j(t) = \int \mathrm{d}^3\mathbf{r}\, u_1^*(\mathbf{r})\hat{\psi}(\mathbf{r},t) \tag{19.46}$$

and $[c_i, c_k^\dagger] = \delta_{j,k}$. The two mode approximation is good provided ε is small, equivalently if $\Omega << \omega_0$. Numerical calculations indicate that the two mode approximation can be acceptable even for such small values as $q_0/r_0 = 3$. With eh two mode expansion the full many body Hamiltonian may be approximated by [25]

$$\hat{H}_2 = E_0(c_1^\dagger c_1 + c_2^\dagger c_2) + \frac{\hbar\Omega}{2}(c_1 c_2^\dagger + c_2 c_1^\dagger) + \hbar\kappa\left((c_1^\dagger c_1)^2 + (c_2^\dagger c_2)^2\right) \tag{19.47}$$

where $\kappa = U_0/2\hbar V_{\mathrm{eff}}$ and $V_{\mathrm{eff}}^{-1} = \int \mathrm{d}^3\mathbf{r}|u_0(\mathbf{r})|^4$ is the inverse effective mode volume of each well. Neglected terms are of order ε^2.

This approximate Hamiltonian is expected to be valid so long as the atomic interactions are not so large as to cause large deviations between the single particle localised states and the true stationary state of the condensate in each well. In practice this means a restriction on atomic number such that $N << \frac{r_0}{|a_0|}$. If we use $r_0 = 5\,\mu\mathrm{m}$ and $a_0 = 5\,\mathrm{nm}$, an atom number as $N = 100$ satisfies the condition. Recently a number of experiments have begun to explore this low atomic number region where quantum fluctuations in the field are dominant, as we discuss on more detail below.

19.7.1 Semiclassical Dynamics

Before proceeding to the full quantum analysis of the two-mode Hamiltonian we first consider the mean-field approximation. For this we employ the Hartree approximation for a fixed number of atoms N, and write the atomic state vector as

$$|\Psi_N(t)\rangle = \frac{1}{\sqrt{N!}}\left[\int \mathrm{d}^3\mathbf{r}\phi_N(\mathbf{r},t)\hat{\psi}^\dagger(\mathbf{r},0)\right]^N |0\rangle \ , \tag{19.48}$$

where $|0\rangle$ is the vacuum. The self-consistent nonlinear Schrödinger equation or Gross-Pitaevskii equation for the condensate wave function $\phi_N(\mathbf{r},t)$ follows from the Schrödinger equation $i\hbar|\dot{\Psi}_N(t)\rangle = \hat{H}(0)|\Psi_N(t)\rangle$, and is given by

$$i\hbar\frac{\partial\phi_N}{\partial t} = \left[-\frac{\hbar^2}{2m}\nabla^2 + V(\mathbf{r}) + NU_0|\phi_N|^2\right]\phi_N \ . \tag{19.49}$$

For a particular choice of the global potential $V(\mathbf{r})$, (19.49) can be solved numerically for a given initial condition. In particular, this equation allows simulations of condensate tunnelling to be performed without the limitations imposed by the two-mode approximation.

In the two-mode approximation we use the local modes described above and write

$$\phi_N(\mathbf{r},t) = \mathrm{e}^{-\mathrm{i}E_0 t/\hbar}[b_1(t)u_1(\mathbf{r}) + b_2(t)u_2(\mathbf{r})] \ . \tag{19.50}$$

Then, to first-order in ε we obtain the coupled-mode equations

$$\frac{\mathrm{d}b_j}{\mathrm{d}t} = -\frac{i\Omega}{2} b_{3-j} - 2i\kappa N |b_j|^2 b_j \ , \tag{19.51}$$

The number of atoms in the jth well is given by

$$N_j(t) = \langle \Psi_N(t) | \hat{c}_j^\dagger \hat{c}_j | \Psi_N(t) \rangle = N |b_j(t)|^2 \ , \tag{19.52}$$

and this provides the link between the coupled-mode amplitudes and the expectation values of the quantum problem.

The coupled-mode (19.51) have an exact solution [15]. For the case that all N atoms are initially localised in well 1, $N_1(0) = N|b_1(0)|^2 = N$, the number of atoms in well 1 varies in time as

$$N_1(t) = \frac{N}{2}\left[1 + cn(\Omega t | N^2/N_c^2)\right] \ , \tag{19.53}$$

with $N_1(t) + N_2(t) = N$. Here $cn(\phi|m)$ is a Jacobi elliptic function, and N_c is the critical number of atoms given by

$$N_\mathrm{c} = \frac{\Omega}{\kappa} \ . \tag{19.54}$$

For $N < N_\mathrm{c}$ this solution exhibits complete and periodic oscillations between the two condensates with a period $K(N^2/N_\mathrm{c}^2)$ which depends on the number of atoms, where $K(m)$ is a complete elliptic integral of the first kind. For $N << N_\mathrm{c}$, cn becomes cos, and the oscillations are precisely like those in the Josephson effect. As the number of atoms is increased the oscillation period increases, until at $N = N_\mathrm{c}$ the period is infinite. This marks a bifurcation in the nonlinear system and at this point the system asymptotically evolves to equal number of atoms $N/2$ in each well. For $N > N_\mathrm{c}$ the period of oscillation reduces again but the exchange between the wells is no longer complete. That is, the coherent tunnelling oscillations are inhibited at high numbers of atoms, and this is the analogue of the self-trapping transition [15] for the double-well BEC. Note that this result arises even for a fixed number of atoms N, and does not therefore rely on coherence between different number states. It does, however, require there to be a well defined relative phase between the amplitudes $b_{1,2}$ of the two potential wells.

We can equally well write the solution in terms of three real variables x, y, z defined by

$$x = \frac{1}{2}(|b_2|^2 - |b_1|^2) \tag{19.55}$$

$$y = -\frac{i}{2}(b_1^* b_2 - b_2^* b_1) \tag{19.56}$$

$$z = \frac{1}{2}(b_1^* b_2 + b_1 b_2^*) \tag{19.57}$$

with $x^2+y^2+z^2=1/4$, so that the dynamics is constrained to the surface of a sphere. We can gain some further insight into the nature of the nonlinear dynamics by considering the fixed points of this dynamical system, that is, those points for which the velocity vanishes ($\dot{x}=\dot{y}=\dot{z}=0$). There are four fixed points, (x^*,y^*,z^*) given by

$$(x^*,y^*,z^*)=\begin{cases}(0,0,\frac{1}{2}) & (1)\\ (0,0,-\frac{1}{2}) & (2)\\ \frac{1}{4}(\sqrt{4\Theta^2-1},0,1)\Theta & (3)\\ \frac{1}{4}(-\sqrt{4\Theta^2-1},0,1)\Theta & (4)\end{cases} \tag{19.58}$$

where $\Theta=\kappa N/\Omega$. If we linearise the motion around each fixed point we see that the resultant eigenvalues for each of the four fixed points above are

$$\begin{aligned}\lambda_1 &= \pm\sqrt{2\Theta-1}\\ \lambda_2 &= \pm i\sqrt{2\Theta+1}\\ \lambda_{3,4} &= \pm i\sqrt{4\Theta^2-1}\end{aligned}$$

The bifurcation at $\Theta=1/2$ is thus a pitchfork bifurcation. For $\Theta<1/2$ there are two elliptic fixed points at the top and bottom of the sphere. Above the bifurcation, $\Theta>1/2$, the elliptic fixed point at the top of there sphere becomes a saddle point, giving rise to two elliptic fixed points that move from the north pole towards the equator at $x=\pm 1/2$. The bifurcation diagram is shown in Fig.19.5.

An experimental demonstration of the transition between tunneling and self trapping was published by the Oberthaler group in 2006 [16]. The double well system was created using an optical dipole standing wave potential superimposed on a magnetic harmonic trap. The potential formed in one dimension has the form

$$V_{\rm dw}=\frac{1}{2}m\omega_x^2(x-\Delta x)^2+V_0\cos^2\left(\frac{\pi x}{d_l}\right) \tag{19.59}$$

where Δx is a relative offset that controls the asymmetry of the potential: when $\Delta x=0$, a symmetric double well is obtained. The parameters of the system were carefully determined by independent measurement to be $\omega_x=2\pi\times 78\,{\rm Hz}$, $V_0=h\times 412\,{\rm Hz}$ and $d_l=5.18\,\mu{\rm m}$ There is harmonic confinement in the other two dimensions. The atoms used were ^{87}Rb. The atomic number varies from one preparation to another but is of the order of $N=1000$. At the start of a run the parameter Δx is set to initialise a particular population difference $z=(N_l-N_r)/(N_l+N_r)$ between a left and right well. In the experiment the self trapping region of phase space requires a critical population difference $z_{\rm c}=0.39$, that is to say Josephson-like tunneling between the wells is apparent when the initial condition is set at $z<z_{\rm c}$, while self trapping results for $z>z_{\rm c}$. After the preparation of the BEC in the asymmetric double well, the offset is changed rapidly (faster than the typical tuneling time of 50 ms) to zero to produce a symmetric double well.

The experimental results were described by an extended two-mode model developed by Ananikian and Bergeman [17]. A comparison of the extended two-mode

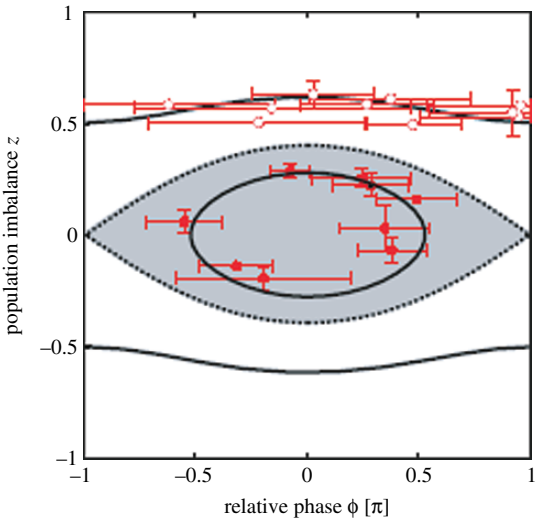

Fig. 19.6 A comparison of theoretically determined phase-portrait of the extended two mode model and the experimental conditions for self trapping and tunneling oscillations for a BEC in a double well potential. The Josephson oscillation region is shaded. From Gati et al. Applied Physics B 82, 207 (2006), Fig. 5

model and the experimental results is shown in Fig. 19.6 in terms of the theoretically determined phase space portrait and the experimentally determined parameters for motion inside the separatrix(tunneling) and motion outside the separatrix (self-trapping).

19.7.2 Quantum Dynamics

The two mode Hamiltonian given in (19.47) can be written in terms of the generators of $su(2)$ as

$$H_2 = \hbar\Omega\hat{J}_z + 2\hbar\kappa\hat{J}_x^2 \tag{19.60}$$

with

$$\hat{J}_x = \frac{1}{2}(c_2^\dagger c_2 - c_1^\dagger c_1) \tag{19.61}$$

$$\hat{J}_y = \frac{i}{2}(c_2^\dagger c_1 - c_1^\dagger c_2) \tag{19.62}$$

$$\hat{J}_z = \frac{1}{2}(c_2^\dagger c_1 + c_1^\dagger c_2) \tag{19.63}$$

The corresponding Casimir invariant is related to number conservation:

$$\hat{J}^2 = \frac{\hat{N}}{2}\left(\frac{\hat{N}}{2} + 1\right) \tag{19.64}$$

We will generally work in a Hilbert space subspace in which all states are number eigenstates, and thus we can use the $N/2(N/2+1)$ dimensional representation of su(2). For this reason we have dropped terms that commute with $\hat{N}$ from the Hamiltonian. In this form the Hamiltonian describes a nonlinear top, with a linear precesssion around the z-axis and a nonlinear precession around the x axis. These operators are of course the operator equivalents to the semiclassical variables defined in the previous section.

From the Heisenberg equations of motion we see that the semiclassical equations of motion are found by taking scaled moments of the operator equations and factorising all quadratic product averages, for example $\langle \hat{J}_z \hat{J}_x \rangle / N^2 = \langle \hat{J}_z \rangle \langle \hat{J}_x \rangle / N^2 = xz$. In Exercise 19.2 we show that this approximation becomes good for condensates with $N >> 1$.

The su(2) operators have an obvious interpretations. The operator $\hat{J}_x$ corresponds to particle number difference between localised states. In Exercise 19.2 you are asked to show that in fact it is simply the occupation number representation of the condensate position operator in the two-mode approximation. Likewise we can show that $\hat{J}_y$ represents the condensate momentum while $\hat{J}_z$ represents the particle number difference between the two lowest energy eigenstates of the potential.

We can contrast the quantum and classical dynamics of the two mode condensate by solving the Schrödinger equation in the representation that diagonalises $\hat{J}_z$. This is shown in Fig. 19.7. The semiclassical oscillations are modified by a periodic collapse and revival envelope. For small condensates considered here, the collapse occurs after only a few tunneling oscillations. However in the semiclassical limit of large atomic number, and the collapse and revival times are much larger.

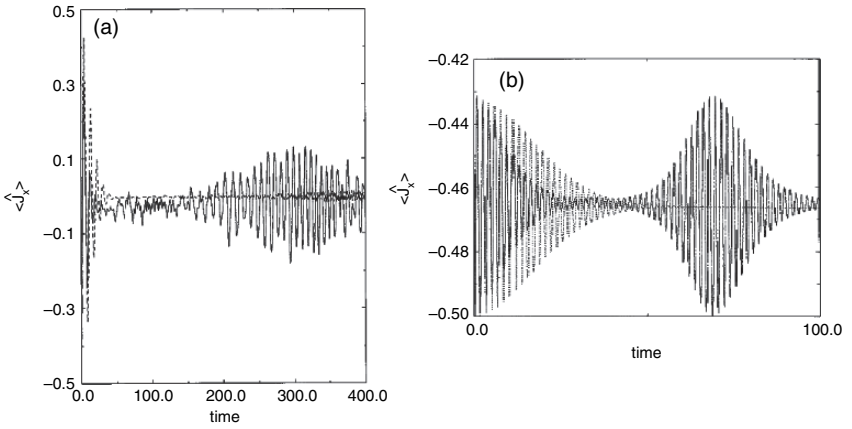

Fig. 19.7 Collapses and revivals in the tunneling oscillations of condensates containing 100 (*solid line*) and 400 atoms (*dashed line*). In (**a**) the number of atoms is such that we are below the critical number $N = 0.9N_c$, while in (**b**) we are above, $N = 2.0N_c$. The time axis has been scaled by $t_0 = 1/\Omega$. From Milburn et al. Phys. Rev. A 55, 4318–4324 (1997) [25]

19.8 Coherence Properties of Bose–Einstein Condensates

The coherence properties of a Bose condensate may be determined in a similar fashion to those for laser light. In a laser first order optical coherence is established via interference experiments and second and higher order optical coherence via intensity correlation measurements.

19.8.1 1st Order Coherence

First order coherence in a Bose-Einstein condensate was established in an experiment demonstrating interference between two condensates [18]. The interference was obtained between two condensates created in a double well trap which were released from the trap and allowed to expand and overlap. The interference fringes observed by absorption imaging are shown in Fig. 19.8. The fringe spacing may be established by considering two point-like condensates with separation d. The relative speed between the two condensates at any point in space is d/t where t is the delay between switching of the trap and observation. The fringe spacing is the de Broglie wavelength λ associated with the relative motion of atoms with mass m,

$$\lambda = \frac{\hbar t}{md} \,. \tag{19.65}$$

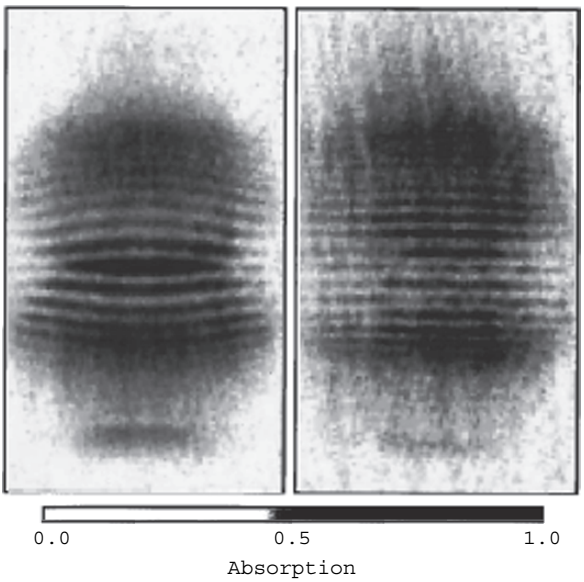

Fig. 19.8 The interference pattern of two expanding condensates released from a trap (Fig. 2 from [18]

Their observation confirmed that the fringe spacing became smaller for larger values of d.

The observed contrast of the atomic interference was between 50 and 100% . Since the condensates are much larger than the observed fringe spacing they must have a high degree of spatial coherence. These measurements established the long range order of the condensate. The theoretical calculations of Sect. 19.6 predicted that two independent condensates will exhibit interference fringes with a phase that varies from run to run. This was not possible to verify in the experiment since mechanical instabilities were sufficient to generate a random phase.

Spatial interference fringes have also been observed between condensate atoms outcoupled from a trap demonstrating that the coherence is preserved by the output coupler. This may be considered as the first prototype of an "atom laser".

19.8.2 Higher Order Coherence

Evidence for *higher–order* coherence, strengthening the analogy between condensates and optical laser photons, has also been provided through careful interpretation of some fundamental condensate properties, in particular, of the loss rate of atoms from the condensate via three–body recombination and of the mean field energy of the condensate.

The atom loss rate due to three–body recombination is directly related to the probability of finding three atoms close to each other [26], and can therefore act as a probe of the third–order correlation function

$$g^{(3)}(\mathbf{r},\mathbf{r},\mathbf{r}) = \frac{\langle \hat{\Psi}^\dagger(\mathbf{r})\hat{\Psi}^\dagger(\mathbf{r})\hat{\Psi}^\dagger(\mathbf{r})\hat{\Psi}(\mathbf{r})\hat{\Psi}(\mathbf{r})\hat{\Psi}(\mathbf{r})\rangle}{n(\mathbf{r})^3} , \tag{19.66}$$

where $n(\mathbf{r}) = \langle \hat{\Psi}^\dagger(\mathbf{r})\hat{\Psi}(\mathbf{r})\rangle$ is the atomic density. Importantly, the value of this function differs between condensates and thermal clouds by a factor of $3! = 6$; in particular, the value of $g^{(3)}(\mathbf{r},\mathbf{r},\mathbf{r})$ for a thermal cloud is a factor of six larger than that for a condensate, implying an atom loss rate due to three–body recombination six times larger. The ratio of the noncondensate to the condensate rate constants for this loss process was found by Burt et al. [27] to be 7.4 ± 2.0, confirming the presence of at least third–order coherence in their condensates.

Similarly, Ketterle and Miesner [28] have pointed out that the mean–field energy of a condensate, $\langle U\rangle$, provides a direct measure of the second–order correlation function,

$$g^{(2)}(\mathbf{r},\mathbf{r}) = \frac{\langle \hat{\Psi}^\dagger(\mathbf{r})\hat{\Psi}^\dagger(\mathbf{r})\hat{\Psi}(\mathbf{r})\hat{\Psi}(\mathbf{r})\rangle}{n(\mathbf{r})^2} , \tag{19.67}$$

through the relationship (see 19.5)

$$\langle U\rangle = \left(\frac{2\pi\hbar^2 a}{m}\right) g^{(2)}(0) \int \mathrm{d}^3 r \, [n(\mathbf{r})]^2 , \tag{19.68}$$

where $g^{(2)}(0) \equiv g^{(2)}(\mathbf{r},\mathbf{r})$, assuming that $g^{(2)}(\mathbf{r},\mathbf{r}')$ depends only on $\mathbf{r}-\mathbf{r}'$. Re–analysing condensate data from earlier experiments, they obtain values of $g^{(2)}(0)$ close to 1, as expected for a condensate and differing from that of a thermal cloud, for which $g^{(2)}(0)=2$. The reduced value of $g^{(2)}(0)$ for a condensate reflects reduced density fluctuations, in direct analogy with the reduced intensity fluctuations of a (photon) laser in comparison with a thermal light source.

We note that $g^{(2)}(0)=1, g^{(3)}(0)=1$, while consistent with a coherent state does not distinguish from a number state for $g^{(2)}(0)=1-1/n, g^{(3)}(0)=1-3/n$ for $n\sim 10^6$.

A direct experimental determination of the atom counting statistics may be made by out coupling atoms from the condensate and letting them fall under the action of gravity: that is an *atom laser*. The atoms fall through an optical cavity and modulate the transmission of a coherent laser beam through the cavity by changing the

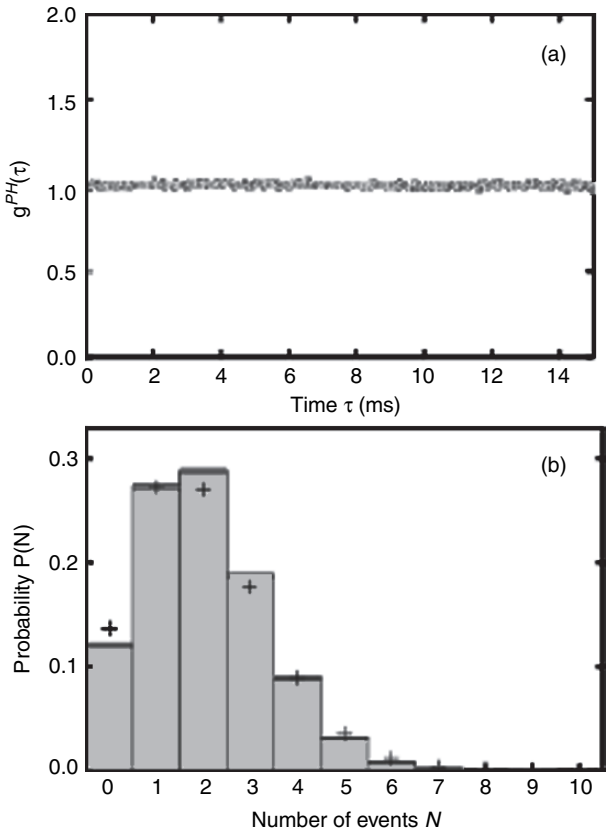

Fig. 19.9 The atom number counting statistics for an out-coupled BEC. In (**a**) the second order correlation functions is shown. (b) the full counting statistics for the atomic number counted in a time $T-1.5$ ms. The symbol + indicates the probability for a Poisson distribution with the same mean number $\bar{n}=1.99$ is shown (Fig. 3 from [22])

absorption and refractive index of the cavity. In the experiment of Öttl et al. [22], using an out-coupled ^{87}Rb BEC, single atoms transiting the driven cavity resulted in a drop in transmission. In this way a Hanbury-Brown Twiss experiment can be done to determine not only $g^{(2)}$ for the atoms but the full counting statistics. The results are shown in Fig. 19.9. We can clearly see the expected value of 1 indicating a coherent beam.

Exercises

19.1. Show that the condensate Hamiltonian is invariant under the gauge transformation $\hat{\psi}(r) \rightarrow \hat{\psi}(r)\mathrm{e}^{\mathrm{i}\phi(r)}$.

19.2. The spin coherent states are defined by (see Exercise 15.3)

$$|\alpha\rangle = (1+|\alpha|^2)^{-j} \sum_{m=-j}^{j} \binom{N}{m}^{1/2} \alpha^{(m+j)} |j,m\rangle \tag{19.69}$$

where $|j,m\rangle$ is the simultaneous eigenstate of $\hat{J}^2$ and $\hat{J}_z$ and α is a complex number. These states have the same form as the general total number eigenstate for a two-mode condensate given in (19.14) and with the operator correspondence given in Sect. 19.7.2. Compute the moments $\langle \hat{J}_k \rangle \quad k = x,y,z$ in terms of α, and show that α lies in the complex plane of the stereographic projection of the Bloch sphere. Also compute the second order moment $\langle \hat{J}_z \hat{J}_x \rangle / N^2$ and show that for $N >> 1$ it may be factorised.

19.3. Show that the occupation number representation of the position operator $\hat{x}$ in the two-mode approximation is given by

$$\hat{x} = \frac{2q_0}{N} \hat{J}_x \tag{19.70}$$

References

1. S.N. Bose: Z. Phys. **26**, 178 (1924)
2. A. Einstein: Sitzber. Kgl. Preuss. Akad. Wiss. 3 (1925)
3. M.H. Anderson, J.R. Ensher, M.R. Matthews, C.E. Wieman, E.A. Cornell: 1995, Science **269**, 198 (1995)
4. K.B. Davis, M.-O. Mewes, M.R. Andrews, N.J. van Druten, D.S. Durfee, D.M. Kurn, W. Ketterle: Phys. Rev. Lett. **75**, 3969 (1995)
5. C.C. Bradley, C.A. Sackett, J.J. Tollett, R.G. Hulet: Phys. Rev. Lett. **75**, 1687 (1995)
6. Fried, D.G., T.C. Killian, L. Willmann, D. Landhuis, S.C. Moss, D. Kleppner, T.J. Greytak: Phys. Rev. Lett. **81**, 3811 (1998)
7. A. Robert, O. Sirjean, A. Browaeys, J. Poupard, S. Nowak, D. Boiron, C.I. Westbrook, A. Aspect: Science, **292**, 461 (2001)

8. R. Wynar, R.S. Freeland, D.J. Han, C. Ryu, D.J. Heinzen: Science **287**, 1016 (2000)
9. M.W. Zwierlein, C.A. Stan, C.H. Schunck, S.M.F. Raupach, A.J. Kerman, W. Ketterle: Phys. Rev. Lett. **92**, 120403 (2004)
10. C. Chin, Andrew J. Kerman, V. Vuleti, S. Chu: Phys. Rev. Lett. **90**, 033201 (2003)
11. C.A. Regal, M. Greiner, D.S. Jin: Phys. Rev. Lett. **92**, 040403 (2004)
12. O. Mandel, M. Greiner, A. Widera, T. Rom, T.W. Hnsch, I. Bloch: Nature, **425**, 937–940 (2003)
13. E.M. Lifshitz, L.P. Pitaevskii: Statistical Physics, Part II (Pergamon, Oxford 1980)
14. J.A. Dunningham, M.J. Collett, D.F. Walls: Phys. Lett. A, **245**, 49 (1998)
15. J.C. Eilbeck, P.S. Lomdahl, A.C. Scott: Physica D, **16**, 318 (1985)
16. R. Gati, M. Albiez, J. Fölling, B. Hemmerling, M.K. Oberthaler: Appl. Phys. B **82**, 207 (2006)
17. D. Ananikian, T. Bergeman: Phys. Rev.A, **73**, 013604 (2006)
18. M.R. Andrews, C.G. Townsend, H.-J. Miesner, D.S. Durfee, D.M. Kurn, W. Ketterle: Science **275**, 637 (1997)
19. M.J. Steel, M.J. Collett: Phys. Rev. A *57*, 2920 (1998)
20. M. Lewenstein, L. You: Phys. Rev. Lett. 77, 3489 (1996b)
21. E.M. Wright, D.F. Walls, J.C. Garrison: Phys. Rev. Lett. **77**, 2158 (1996)
22. A. Öttl, S. Ritter, M.l Köhl, and T. Esslinger, Phys. Rev. Letts., 95, 090404 (2005)
23. J. Javanainen, S.M. Yoo: Phys. Rev. Lett. **76**, 161 (1996)
24. T. Wong, M.J. Collett, D.F. Walls: Phys. Rev. A **54**, R3718 (1996)
25. G.J. Milburn, J. Corney, E.M. Wright, D.F. Walls, Phys. Rev A. **55**, 4318 (1997)
26. Yu. Kagan, B.V. Svistunov, G.V. Shlyapnikov: JETP Lett. **42**, 209 (1985)
27. E.A. Burt, R.W. Ghrist, C.J. Myatt, M.J. Holland, E.A. Cornell, C.E. Wieman: Phys. Rev. Lett. 79, 337 (1997)
28. W. Ketterle, H.-J. Miesner: Phys. Rev. A **56**, 3291 (1997)

Further Reading

J.R. Anglin, W. Ketterle: Bose-Einstein Condensation of Atomic Gases, Nature, **416**, 211 (2002)
A. Leggett: Bose-Einstein Condensation in the Alkali Gases, Rev. Mod. Phys. **73**, 307 (2001)
F. Dalfovo, S. Giorgini, L.P.Pitaevskii, S. Stringari: Theory of Bose-Einstein Condensation in Trapped Gases, Rev. Mod. Phys. **71**, 463 (2001)
I. Bloch: Ultracold Quantum Gases in Optical Lattices, Nat. Phys. **1**, 23 (2005)
A.S. Parkins, D.F. Walls: Bose-Einstein condensation in Dilute Atomic Vapors, Phys Rep. **303**, 1 (1998)